Journal of Sound and Vibration (2000) **236**(3), 375–400
doi:10.1006/jsvi.1999.2992, available online at http://www.idealibrary.com on IDEAL®

ERRORS ARISING FROM THREE-DIMENSIONAL ENERGY DENSITY SENSING IN ONE-DIMENSIONAL SOUND FIELDS

B. S. Cazzolato† and C. H. Hansen

Department of Mechanical Engineering, University of Adelaide, SA, 5005, Australia

(*Received* 4 *June* 1999, *and in final form* 6 *September* 1999)

The performance of four different configurations of three-dimensional acoustic energy density sensors are evaluated for two idealized one-dimensional sound field: a reactive single mode and a propagating plane wave. The 4 configurations of sensors are; two types of 4-microphone arrangements, a 6-microphone arrangement and a 7-microphone arrangement. Like the companion paper for one-dimensional sensors by the same authors this paper investigates the bias errors arising from four error types: inherent, phase mismatch, sensitivity mismatch and spatial errors. It is shown that for plane wave conditions a 4-microphone arrangement is more accurate than the "standard" 6-microphone arrangement.

1. INTRODUCTION

The purpose of the study described here was to investigate various physical configurations of three-axis energy density sensors for use in active noise control systems. Selection of error sensors for ANC are typically driven by cost, simplicity and size and this study was no exception. It will be shown that an effective three-axis energy density sensor can be implemented using only 4-microphones rather than 6-microphones as used in previous sensors [1, 2] and although there is a noticeable reduction in accuracy in energy density measurement, it has been shown that active energy density control is extremely robust and insensitive to the various errors that occur [3, 4]. Subsequently, it is concluded that the degradation in accuracy experienced with the 4-microphone sensor is acceptable for active noise control applications.

The errors arising in the measurement of acoustic energy density by single-axis sensors in one-dimensional sound fields have been derived by Cazzolato and Hansen [5]. In this companion paper, the error analysis will be extended to three dimensions where 4-different three-axis energy density sensors will be analyzed.

Several possible sensor configurations are discussed with the merits of each explained. The measurement of energy density is discussed briefly and a strategy for the estimation of the errors arising from the sensors is then derived. Unlike the one-dimensional sensors it is not possible to derive analytical expressions for the errors in the energy density estimate and therefore the errors are solved numerically.

The measured errors in energy density from the 4 configurations arising from the finite-difference and finite-sum approximations, phase mismatches, sensitivity mismatches and spatial manufacturing defects are derived. It will be shown that the energy density in

† Now at the Institute of Sound and Vibration Research, University of Southampton, Southampton SO17 1BJ, England.

0022-460X/00/380375 + 26 $35.00/0

three dimensions can be measured adequately with 4 microphones rather than the conventional 6 used in previous sensors. It is also argued that if an extremely accurate measure of energy density is required a 7-microphone sensor should be used. This has less than half the error of a 6-microphone sensor of the same dimensions.

2. 3-D ENERGY DENSITY SENSOR CONFIGURATIONS

The time-averaged acoustic energy density at a point $\mathbf{x}$ is defined as the sum of the acoustic potential energy density and the acoustic kinetic energy density at $\mathbf{x}$ and is given [5] as

$$E_D(\mathbf{x}) = \frac{\bar{p}^2(\mathbf{x})}{2\rho c^2} + \frac{\rho \bar{v}^2(\mathbf{x})}{2} = \frac{1}{4\rho c^2}\left[p^2(\mathbf{x}) + (\rho c v)^2(\mathbf{x})\right], \tag{1}$$

where p and v are the peak amplitudes of the acoustic pressure and total particle velocity at $\mathbf{x}$, respectively, the overbar represents the time-averaged quantities of the pressure and particle velocity, ρ is the density of sound and c is the speed of sound. The velocity term includes all three orthogonal velocity components, i.e., $v(\mathbf{x}) = iv_x(\mathbf{x}) + jv_y(\mathbf{x}) + kv_z(\mathbf{x})$.

Four configurations of three-axis energy density sensors have been considered in the numerical study. The first and most common sensor is a 6-microphone sensor used by Sommerfeldt *et al.* [1] and Parkins *et al.* [2]. This consists of three pairs of microphones separated by a distance $2h$, on three orthogonal axes and is shown in Figure 1. It should be

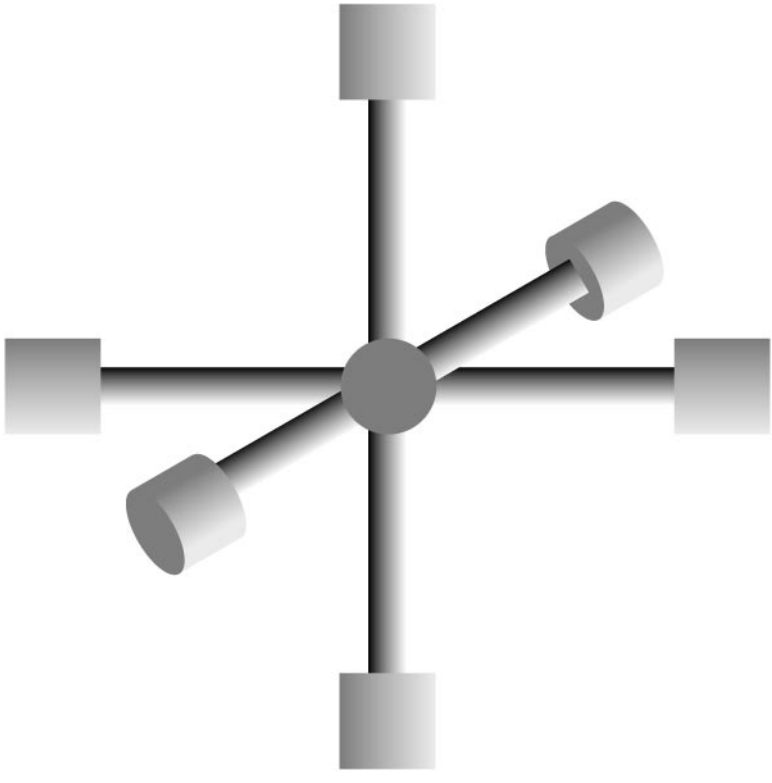

Figure 1. Energy density sensor using 6 or 7 microphones.

noted that Sommerfeldt *et al.* [1] and Parkins *et al.* [2] mounted the microphones within a sphere (rather than as shown in Figure 1) in an attempt to use the effects of diffraction caused by the sensor [6] to produce more favourable bias conditions, and in doing so reduce the inherent errors. Therefore compared to the "suspended" 6-microphone arrangement shown in Figure 1, the hard sphere allowed the sensor to either be reduced in size by two-thirds or to extend the upper frequency range by 50%. It should be noted, however, that the instrumentation errors which affect the low-frequency limit were found to be higher for the rigid sphere arrangement, and therefore the benefits of the rigid sphere tend to be negated. The pressure estimated by the 6-microphone arrangement used in the simulations here is the mean of that sensed by each of the 6 microphones. The velocity for each axis was calculated using the following expression [5]:

$$v(t, \mathbf{x}) \approx -\frac{1}{2h\rho} \int [p(t, \mathbf{x}_2) - p(t, \mathbf{x}_1)] \, \mathrm{d}t, \tag{2}$$

where $2h$ is the distance separating the acoustic centres of the microphones, commonly referred to as the *separation distance*. The "acoustic centre" or "measurement point" is given by the geometric centre of the sensor and the pressure was calculated by taking the mean of all six pressure measurements.

The second sensor, a 7-microphone configuration, was a variation of the first. The additional microphone was located at the geometric centre of the 6-microphone sensor to measure the pressure for the sensor (see Figure 1). By measuring the pressure directly rather than interpolating, the error in pressure associated with the finite sum was avoided.

The third energy density sensor was a 4-microphone configuration as shown in Figure 2. Three microphones (marked x, y and z), each forming one of the ends of the three orthogonal axes (marked x, y and z), were located on a circle 120° apart. The origin of the sensor was located on the normal to the plane of the circle and passing through the centre of the circle. The distance from the centre microphone (microphone o) to the other microphones was $2h$. The pressure sensed by the centre microphone was used as the pressure for the sensor. The particle velocities were calculated using equation (2). It should be noted that with this arrangement the particle velocity components are effectively measured at three different locations, each being at the bisector of the line formed by the microphone pairs. Therefore, the resulting particle velocity vector is determined from three components that do not originate at one location. In a field of plane propagating waves it will be shown that this does not matter. However, in a reactive environment such a configuration does introduce an error which is dependent upon the orientation of the sensor to the sound field.

The advantage of this design is that less signal conditioning channels are required compared to the 6- and 7-microphone sensors. The current design was arrived at independently, although the concept of a 4-microphone sensor to measure the acoustic energy density is not new. Schumacher and Hixson [7] presented a paper on a four-microphone orthogonal array used to measure the energy density in reverberant and semi-reverberant sound fields. The authors also found in [8] a similar configuration used for the measurement of acoustic intensity. The application of such a design for the measurement of acoustic intensity is highly questionable due to the significant phase errors (in both the pressure and velocity estimate) arising from the non-coincident measurement locations of the pressure and particle velocity estimate. Since the calculation of sound intensity requires the product between the pressure and particle velocity to be taken, and when these are in quadrature or close to quadrature, such as in a reactive sound field, any small error in phase between the pressure and particle velocity leads to a large error in the

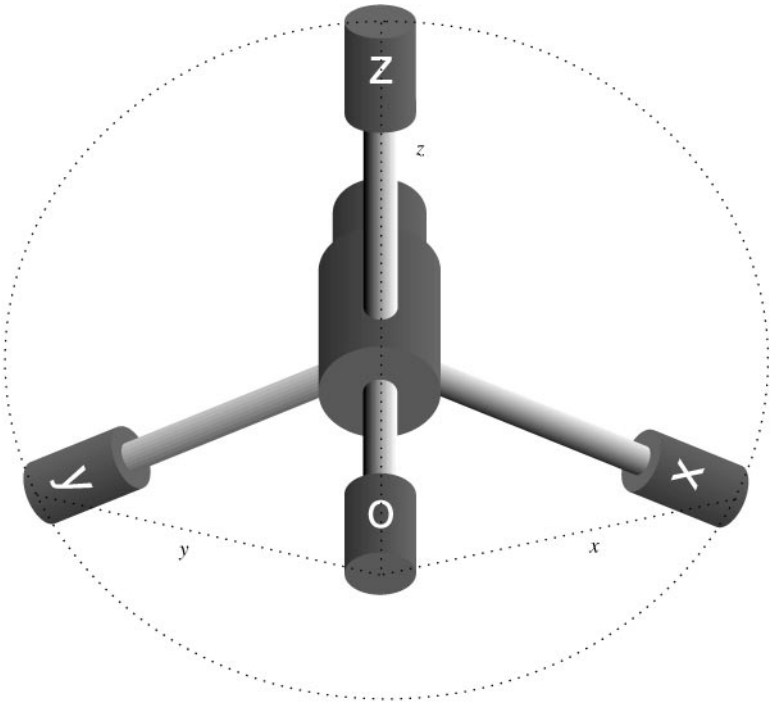

Figure 2. 4 Microphone three-axis energy density sensor.

active sound intensity. However, for the measurement of energy density it will be shown that the design is adequate since the calculation of acoustic energy density takes the sum of the squares of the pressure and article velocity, and therefore is only susceptible to errors in magnitudes of the two components.

It is worth noting that this design has two advantages over the two earlier designs. The most obvious advantages is that less signal conditioning and less channels are required thus reducing the cost and complexity of the unit and making calibration easier. The other advantage is associated with installation. The plane formed by the three circumferentially located microphones of the 4-microphone sensor sits flush against surfaces whereas it is not so neat with the 6/7-microphone sensor. Although there is little point in mounting an energy density sensor adjacent to a rigid wall since the particle velocity is inherently zero, they may also be mounted against less rigid surfaces such as the head-rests of vehicle seats. The more compact design of the 4-microphone sensor lends itself to such applications more readily.

The fourth configuration of energy density sensor investigated was an adaptation of the 4-microphone sensor. Rather than using the pressure at the "centre microphone", the mean pressure sensed by the 4 microphones was used as the pressure for the sensor. It will be shown that, by making the "origin" of the sensor equal to the geometric centre, the inherent errors in reactive sound field are reduced. The particle velocities were calculated as before.

For all the following calculations, it has been assumed the microphones were omni-directional. Other effects such as diffraction have also been neglected. This assumption is valid for the frequency range of interest for active noise control applications of such sensors.

3. ERRORS IN THE MEASUREMENT OF ACOUSTIC ENERGY DENSITY WITH 3-D SENSORS

For single-axis energy density sensors the error analysis is relatively simple and analytical expressions can easily be derived. Deriving expressions for the energy density for the three-axis sensors is not so straightforward, since it is not only the position within the field which influences the accuracy but also the orientation of the sensor within the field. Therefore, numerical integration has been used to calculate the accuracy of each sensor as follows.

1. Define the pressure field.
2. Define the original positions of the microphones.
   (a) Apply a spatial error if required.
3. Select the position of the sensor within the field (not necessary for a plane wave).
4. Apply a co-ordinate transformation (rotation and translation).
5. Calculate the pressure at each microphone.
6. Apply the following instrumentation corrections to the measured pressures if required.
   (a) Phase mismatch.
   (b) Sensitivity error.
7. Calculate the pressure and velocity vectors for the sensor.
8. Using the results from step 7 calculate the ED measured by the sensor for the particular orientation.
9. Repeat from steps 2(a) to 8 for all possible angles and positions.
10. Sum (integrate) the results and calculate the "average" error.

3.1. ERROR ANALYSIS

It will be shown that the errors arising from the measurement of the energy density in three dimensions are similar to those arising in one dimensions [5]. At the high-frequency limit, the errors associated with the three-dimensional sensors are of similar magnitude but typically less than those of the one-dimensional sensor arrangements. However, the errors associated with the three-dimensional sensor arrangements at the low-frequency limit are typically three times larger than for the one-dimensional sensors.

3.1.1. *Original position matrices*

For the 4-microphone sensor, it can be shown that the positions of the microphones relative to the centre of the circle formed by the three planar microphones, with the z-axis of the Cartesian co-ordinate system in the direction of the out-of-plane microphone, is given by the following matrix:

$$\hat{\mathbf{X}}_4 = \begin{bmatrix} 0 & \dfrac{-h2\sqrt{2}}{\sqrt{3}} & \dfrac{h\sqrt{2}}{\sqrt{3}} & \dfrac{h\sqrt{2}}{\sqrt{3}} \\ 0 & 0 & h\sqrt{2} & -h\sqrt{2} \\ \dfrac{h2}{\sqrt{3}} & 0 & 0 & 0 \end{bmatrix}. \tag{3}$$

Unlike the centre of the 6-microphone sensor which lies at the bisector of all 3 microphone pairs, the "centre" of the 4-microphone sensor is not immediately apparent

since neither the pressure nor the particle velocity components are measured at coincident locations. Therefore, as is the case for the 6-microphone sensor, the geometric centre of the 4-microphone sensor (defined as the mean of all four positions) will be used as the "centre", is

$$\mathbf{X}_0 = \begin{bmatrix} 0 & \frac{-h2\sqrt{2}}{\sqrt{3}} & \frac{h\sqrt{2}}{\sqrt{3}} & \frac{h\sqrt{2}}{\sqrt{3}} \\ 0 & 0 & h\sqrt{2} & -h\sqrt{2} \\ \frac{h2}{\sqrt{3}} & 0 & 0 & 0 \end{bmatrix} \begin{bmatrix} \frac{1}{4} \\ \frac{1}{4} \\ \frac{1}{4} \\ \frac{1}{4} \end{bmatrix} = \begin{bmatrix} 0 \\ 0 \\ \frac{h2}{\sqrt{3}} \end{bmatrix} \tag{4}$$

Therefore, the position vector for the 4-microphone sensor from the geometric centre of the sensor is given by $\mathbf{X}_4 = \hat{\mathbf{X}}_4 - \mathbf{X}_0$, i.e.,

$$\mathbf{X}_4 = \begin{bmatrix} 0 & \frac{-h2\sqrt{2}}{\sqrt{3}} & \frac{h\sqrt{2}}{\sqrt{3}} & \frac{h\sqrt{2}}{\sqrt{3}} \\ 0 & 0 & h\sqrt{2} & -h\sqrt{2} \\ \frac{h\sqrt{3}}{2} & -\frac{h}{2\sqrt{3}} & -\frac{h}{2\sqrt{3}} & -\frac{h}{2\sqrt{3}} \end{bmatrix}. \tag{5}$$

For the other two geometric configurations of energy density sensors, the location of each element of the sensors are defined by the position matrices

$$\mathbf{X}_6 = \begin{bmatrix} -h & h & 0 & 0 & 0 & 0 \\ 0 & 0 & -h & h & 0 & 0 \\ 0 & 0 & 0 & 0 & -h & h \end{bmatrix} \tag{6}$$

and

$$\mathbf{X}_7 = \begin{bmatrix} -h & h & 0 & 0 & 0 & 0 & 0 \\ 0 & 0 & -h & h & 0 & 0 & 0 \\ 0 & 0 & 0 & 0 & -h & h & 0 \end{bmatrix} \tag{7}$$

where $\mathbf{X}_6$ and $\mathbf{X}_7$ which correspond to the 6- and 7-element sensor respectively. The spacing between all microphone pairs for all three configurations is $2h$.

3.1.2. *Co-ordinate transforms*

Since the orientation and the location of the sensors in the sound field influences the magnitude of the energy density error it was essential that all angles and positions of the sensor relative to the sound field were investigated. This involved the application of a rotation matrix followed by a translation matrix.

The original position of each sensor was rotated, first by an amount α about the z-axis, followed by a rotation β about the y-axis and finally a rotation γ about the x-axis. Combining the three basic rotation matrices into a single rotation matrix by performing

successive matrix multiplications leads to

$$\mathbf{R} = \begin{bmatrix} C_\alpha C_\beta & -S_\alpha C_\beta & S_\beta \\ (S_\alpha C_\gamma + C_\alpha S_\beta S_\gamma) & (C_\alpha C_\gamma + S_\alpha S_\beta S_\gamma) & -C_\beta S_\gamma \\ (S_\alpha S_\gamma - C_\alpha S_\beta C_\gamma) & (C_\alpha S_\gamma + S_\alpha S_\beta C_\gamma) & C_\beta C_\gamma \end{bmatrix}, \tag{8}$$

where C and S represent the cosine and sine respectively. Each sensor element was then displaced by a displacement column vector

$$\Delta\mathbf{x}_i = \begin{bmatrix} x \\ y \\ z \end{bmatrix}. \tag{9}$$

Therefore, the final expression for the orientation and position of the sensor elements is given by the following transform:

$$\hat{\mathbf{X}}_i = \mathbf{R}\mathbf{X}_i + \Delta\mathbf{X}_i \tag{10}$$

where the subscript i refers to the number of elements in the sensor and $\Delta\mathbf{X}_i$ is the displacement matrix with i columns given by equation (9).

3.1.3. *Spatial errors*

It was shown for single-axis energy density sensors that errors in the geometry of sensors lead to errors in the energy density estimate. To determine the error associated with spatial errors with respect to the original locations, each of the sensor elements was displaced by a small error given by the following:

$$\mathbf{s} = \begin{bmatrix} s_x \\ s_y \\ s_z \end{bmatrix}. \tag{11}$$

Therefore, rewriting equation (10) for the locations of the sensor elements with respect to the global Cartesian co-ordinate system including the spatial error gives

$$\hat{\mathbf{V}}_i = \mathbf{R}[\mathbf{X}_i + \mathbf{S}_i] + \Delta\mathbf{X}_i, \tag{12}$$

where $\mathbf{S}_i$ is the spatial error matrix with i columns given by equation (11). The spatial error matrix differs from the displacement matrix in that it is applied prior to the rotation of the sensor. In other words, the spatial error remains constant relative to the geometry of the sensor regardless of orientation or location within the sound field.

3.1.4. *Pressure response*

To determine the accuracy of the energy density estimate provided by the four energy density sensors, an estimate of the pressures at the sensor microphones is required. This is determined by the pressure operator which is a function of the sound field. In the case of a one-dimensional reactive sound field or a progressive plane wave the pressure operator. P, is given by equations (13) and (14), respectively,

$$P(x, t) = P_0 \cos(k_l x) \qquad P(x, t) = P_0 \mathrm{e}^{-\mathrm{j}kx}, \tag{13, 14}$$

where k_l in equation (13) is the eigenvalue of the mode given by $k_l = n\pi/L$, where n is an integer and L is the length of the cavity. To investigate the effect that wavelength has on the accuracy of the estimates it is prudent to let the length of the cavity increase with frequency such that $L = n\lambda/2$, i.e. $k_l = k$. This then allows a direct comparison with the case of a free propagating wave.

Therefore, the pressure at each microphone position is given by the $(i \times 1)$ pressure column vector

$$\mathbf{p}_i = P(\hat{\mathbf{V}}_i^{\mathrm{T}}). \tag{15}$$

3.1.5. *Phase mismatch errors*

The phase mismatch can be modelled as a temporal rotation in the elements of the sensor, i.e., for the 4-microphone sensor equation (15) becomes

$$\mathbf{p}_i = \mathbf{\Phi}_i P(\hat{\mathbf{V}}_i^{\mathrm{T}}), \tag{16}$$

where $\mathbf{\Phi}_i$ is the phase mismatch matrix (for the 4-microphone sensor) defined by

$$\mathbf{\Phi}_i = \begin{bmatrix} e^{j\phi_1} & 0 & 0 & 0 \\ 0 & e^{j\phi_2} & 0 & 0 \\ 0 & 0 & e^{j\phi_3} & 0 \\ 0 & 0 & 0 & e^{j\phi_4} \end{bmatrix} \tag{17}$$

where ϕ_i is the phase error about some arbitrary reference.

3.1.6. *Sensitivity errors*

The individual microphones may differ in sensitivity which alters both the pressure sum and difference and subsequently the estimated pressure and particle velocity. The pressure estimate can be altered by pre-multiplying the "true" pressure vector by the diagonal sensitivity matrix, $\mathbf{T}_i$, with the diagonal elements of the matrix corresponding to the microphone sensitivities

$$\hat{\mathbf{p}}_i = \mathbf{T}_i \mathbf{p}_i. \tag{18}$$

3.1.7. *Sensor pressure and velocity*

The pressure and velocity (weighted by ρc per equation (1)) of the sensor, given by a 4-element vector $\mathbf{d}$, can be calculated using a linear combination of the individual microphones, i.e.,

$$\mathbf{d} = \mathbf{D}\hat{\mathbf{p}}, \tag{19}$$

where $\mathbf{D}$ is the sensor-dependent $(4 \times n_d)$ pressure to energy density transfer matrix, n_d is the number of microphones per sensor and $\mathbf{d}$ is the (4×1) energy density column vector given by

$$\mathbf{d} = \begin{bmatrix} p \\ \rho c v_x \\ \rho c v_y \\ \rho c v_z \end{bmatrix}. \tag{20}$$

3.1.7.1. 4-*microphone sensor without summer*. The energy density column vector for the 4-microphone sensor without a pressure summer (i.e., the pressure estimate used by the sensor is simply the pressure measured by the origin microphone), is given by

$$\mathbf{d}_4 = \mathbf{D}_4 \hat{\mathbf{p}}_4, \tag{21}$$

where the (4×4) pressure to energy density transfer matrix is

$$\mathbf{D}_4 = \begin{bmatrix} 1 & 0 & 0 & 0 \\ -\dfrac{\mathrm{j}}{2kh} & \dfrac{\mathrm{j}}{2kh} & 0 & 0 \\ -\dfrac{\mathrm{j}}{2kh} & 0 & \dfrac{\mathrm{j}}{2kh} & 0 \\ -\dfrac{\mathrm{j}}{2kh} & 0 & 0 & \dfrac{\mathrm{j}}{2kh} \end{bmatrix}. \tag{22}$$

3.1.7.2. 4-*microphone sensor with summer*. The energy density column vector for the 4-microphone sensor with a pressure summer, i.e., the pressure estimate used by the sensor is the mean of the pressures measured by the 4 microphones, is given by

$$\mathbf{d}_{4_s} = \mathbf{D}_{4_s} \hat{\mathbf{p}}_4, \tag{23}$$

where the (4×4) pressure to energy density transfer matrix is

$$\mathbf{D}_{4_s} = \begin{bmatrix} \dfrac{1}{4} & \dfrac{1}{4} & \dfrac{1}{4} & \dfrac{1}{4} \\ -\dfrac{\mathrm{j}}{2kh} & \dfrac{\mathrm{j}}{2kh} & 0 & 0 \\ -\dfrac{\mathrm{j}}{2kh} & 0 & \dfrac{\mathrm{j}}{2kh} & 0 \\ -\dfrac{\mathrm{j}}{2kh} & 0 & 0 & \dfrac{\mathrm{j}}{2kh} \end{bmatrix}. \tag{24}$$

3.1.7.3. 6-*microphone sensor*. The energy density column vector for the 6-microphone sensor (with a pressure estimate equal to the mean of the 6 microphones) is given by

$$\mathbf{d}_6 = \mathbf{D}_6 \hat{\mathbf{p}}_6, \tag{25}$$

where the (4×6) pressure to energy density transfer matrix is

$$\mathbf{D}_6 = \begin{bmatrix} \dfrac{1}{6} & \dfrac{1}{6} & \dfrac{1}{6} & \dfrac{1}{6} & \dfrac{1}{6} & \dfrac{1}{6} \\ -\dfrac{\mathrm{j}}{2kh} & \dfrac{\mathrm{j}}{2kh} & 0 & 0 & 0 & 0 \\ 0 & 0 & -\dfrac{\mathrm{j}}{2kh} & \dfrac{\mathrm{j}}{2kh} & 0 & 0 \\ 0 & 0 & 0 & 0 & -\dfrac{\mathrm{j}}{2kh} & \dfrac{\mathrm{j}}{2kh} \end{bmatrix}. \tag{26}$$

3.1.7.4. *7-microphone sensor*. The energy density column vector for the 7-microphone sensor (with the pressure of the sensor equal to the centre microphone) is given by

$$\mathbf{d}_7 = \mathbf{D}_7 \hat{\mathbf{p}}_7, \tag{27}$$

where (4×7) pressure to energy density transfer matrix is

$$\mathbf{D}_7 = \begin{bmatrix} 0 & 0 & 0 & 0 & 0 & 0 & 1 \\ -\frac{\mathrm{j}}{2kh} & \frac{\mathrm{j}}{2kh} & 0 & 0 & 0 & 0 & 0 \\ 0 & 0 & -\frac{\mathrm{j}}{2kh} & \frac{\mathrm{j}}{2kh} & 0 & 0 & 0 \\ 0 & 0 & 0 & 0 & -\frac{\mathrm{j}}{2kh} & \frac{\mathrm{j}}{2kh} & 0 \end{bmatrix}. \tag{28}$$

3.1.8. *Energy density*

The time-averaged energy density measured by each sensor is given by the following expression:

$$\bar{E}_D = \frac{1}{4\rho c^2} \mathbf{d}^H \mathbf{d} \tag{29}$$

3.2. SIMULATION RESULTS

A simulation using the procedure outlined above was run to calculate the accuracy of the three-dimensional energy density sensor configurations. The energy density for the 4 sensor configurations was calculated for a one-dimensional reactive sound field and a progressive plane wave. Each of the three orthogonal angles were stepped from 0 to π in steps of $\pi/8$ so as to get a measure of the effect that orientation has on the energy density estimate. The position in the reactive sound field was varied from 0 to $\lambda/2$ in steps of $\lambda/16$. This was unnecessary with the plane wave simulation since the energy density estimate is independent of position. These intervals were found to be sufficient for the error to have converged to 3 significant figures. The following results have been calculated from the simulation.

- Normalized mean-energy density estimate given by

$$\frac{\bar{E}_D}{E_D} = \frac{1}{nE_D} \sum_{i=1}^{n} E_{D_i}, \tag{30}$$

  where $\bar{E}_D$ is the mean energy density measured by the sensor for all possible angles and positions throughout the entire field, E_D is the true energy density throughout the entire field, E_{D_i} is the ith estimate of the energy density at some location and orientation within the field and n is the number of estimates.
- Normalized r.m.s. error about exact ED given by

$$e(E_D)_{r.m.s.} = \frac{1}{E_D} \sqrt{\frac{1}{n} \sum_{i=1}^{n} (E_{D_i} - E_D)^2}. \tag{31}$$

- Normalized standard deviation or square root of the variance which is equal to the expected value of the squared differences of the estimates from the mean ED given by

$$e(\bar{E}_D)_{r.m.s.} = \frac{1}{E_D}\sqrt{\frac{1}{n}\sum_{i=1}^{n}(E_{D_i} - \bar{E}_D)^2}. \tag{32}$$

- Normalized maximum and minimum ED given by

$$\frac{E_{D_{max}}}{E_D} = \max(E_{D_i})/E_D \tag{33}$$

and

$$\frac{E_{D_{min}}}{E_D} = \min(E_{D_i})/E_D \tag{34}$$

respectively.

The mean energy density estimate, equation (30), gives a measure of the average bias error in the energy density from each of the sensors (throughout the entire field). The difference between the estimate and the true value is known as the *bias* of the estimate. The normalized bias is simply the bias divided by the true energy density, i.e., $b(E_D) = (\bar{E}_D - E_D)/E_D$. The r.m.s. error, equation (31), is a measure of the deviation of the estimated energy density from the exact value. This is important when one is using different types of sensors together, for example, a combination of microphones and energy density sensors. The normalized standard deviation or square root of the variance, equation (32), is the portion of the error that is not systematic [9, Section 1.4.3] and gives a measure of the deviation of the estimated energy density experienced during the measurement in a field. This is important when using sensors of the same type in active noise control systems since in active control systems it is desirable to have the control effort weighting the same for all sensors. It can be shown that the r.m.s. error is equal to the square root of the variance plus the square of the bias [9]:

$$e(E_D)_{r.m.s.} = \sqrt{e(\bar{E}_D)^2_{r.m.s.} + \left(\frac{\bar{E}_D}{E_D} - 1\right)^2}. \tag{35}$$

Therefore, if the normalized bias is zero or negligible, then the r.m.s. error and root of the square variance are equal. The maximum and minimum, equation (33) and (34), given an indication of the range of expected values.

3.2.1. *Finite separation errors* (*inherent*)

Using the procedure outlined in section 3.1, the ratios of the exact energy density to the approximation for each sensor are given below.

3.2.1.1. *One dimensional reactive field.* The five measures of the accuracy of the energy density estimate for the four-sensor configurations, as given by equations (30)–(34), are plotted in Figure 3. It is quite apparent that the 6- and 7-microphone configurations outperform the 4-microphone configurations with the exception of the error in the mean (the bias) seen in Figure 3(a), where the 4-microphone sensor without the summer is similar to the 7-microphone configuration. This is because both arrangements do not use a finite sum to approximate the pressure. It can be seen that the r.m.s. error of the 7-microphone

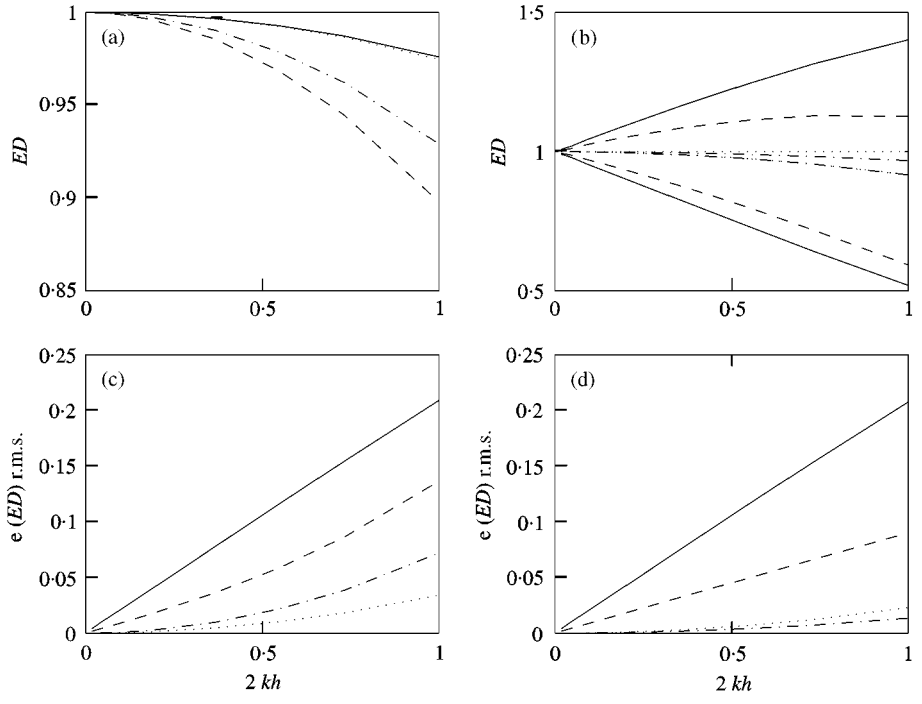

Figure 3. Inherent errors as a function of the non-dimensionalized separation distance $2kh$ in a reactive sound field: (a) normalized mean energy density, (b) normalized maximum and minimum, (c) normalized r.m.s. error and (d) normalized standard deviation. —— 4 Mic; – – 4S Mic; ·–· 6 Mic; ···· 7 Mic.

sensor is half that of the 6-microphone sensor and a quarter that of the 4-microphone sensor with the pressure summer.

A linear regression was performed on the results shown above, where a fifth order polynomial with respect to $2kh$ was fitted to each of the five curves. The polynomials listed below are accurate to 3 significant figures (for $2kh < 1$), and where possible, the coefficients have been expressed as rational number, otherwise the coefficients have been recorded as 3 digit decimal. It was found that the normalized mean energy density for the four energy density sensor configurations converged to the following for large kh:

$$\begin{aligned}\frac{\bar{E}_D}{E_D} &= 1 - 0{\cdot}024\,(2kh)^2, \quad \text{4-microphone probe without summer}\\ &= 1 - 0{\cdot}108\,(2kh)^2, \quad \text{4-microphone probe with summer}\\ &= 1 - 0{\cdot}072\,(2kh)^2, \quad \text{6-microphone probe}\\ &= 1 - 0{\cdot}025\,(2kh)^2, \quad \text{7-microphone probe.}\end{aligned} \tag{36}$$

The normalized mean energy density for the one-dimensional energy density sensor is either $1 - 0{\cdot}167\ (2kh)^2$, or $1 - 0{\cdot}042\ (2kh)^2$, for the two 2- and 3-microphone sensor respectively [5]. The 6-microphone three-dimensional sensor is equivalent to the 2-microphone sensor in one-dimension since the pressure in the centre of the sensor must be estimated, whereas the 7-microphone three-dimensional sensor is equivalent to the 3-microphone sensor in one dimension since the centre pressure is measured directly. It is

interesting to note that on average, both the 6- and 7-microphone sensors perform better in one-dimensional reactive sound fields than their equivalent one-dimensional arrangements. The reason for the 6-microphone 3-D sensor performing better than the 2-microphone sensor is simply that the additional four microphones allow a better estimate of the mean sensor pressure. For example, if the 6-microphone sensor has one if its principle axes aligned with the sound field, then the centre pressure is given by $\hat{p}_0 = \frac{1}{6}\sum_{i=1}^{6} p_i = (p_1 + p_2)/6 + \frac{2}{3}p_0$ whereas the centre pressure of the 2-microphone sensor is given by $\hat{p}_0 = (p_1 + p_2)/2$. Therefore, the inherent error of the 2-microphone sensor in a reactive sound field is approximately 3 times that of the 6-microphone sensor.

The normalized r.m.s. is given by

$$\begin{aligned} e(E_D)_{r.m.s.} &= 0{\cdot}213(2kh), && \text{4-microphone probe without summer} \\ &= 0{\cdot}089(2kh) + 0{\cdot}068(2kh)^3 - 0{\cdot}026(2kh)^4, && \text{4-microphone probe with summer} \\ &= 0{\cdot}073(2kh)^2, && \text{6-microphone probe} \\ &= 0{\cdot}034(2kh)^2, && \text{7-microphone probe,} \end{aligned} \tag{37}$$

The normalized standard deviation is given by

$$\begin{aligned} e(\bar{E}_D)_{r.m.s.} &= 0{\cdot}213(2kh), && \text{4-microphone probe without summer} \\ &= 0{\cdot}090(2kh), && \text{4-microphone probe with summer} \\ &= 0{\cdot}014(2kh)^2, && \text{6-microphone probe,} \\ &= 0{\cdot}023(2kh)^2, && \text{7-microphone probe,} \end{aligned} \tag{38}$$

The maximum normalized energy density estimate is

$$\begin{aligned} \frac{E_{D_{max}}}{E_D} &= 1 + 0{\cdot}480(2kh), && \text{4-microphone probe without summer} \\ &= 1 + 0{\cdot}295(2kh) - 0{\cdot}150(2kh)^2, && \text{4-microphone probe with summer} \\ &= 1 - 0{\cdot}031(2kh)^2, && \text{6-microphone probe} \\ &= 1, && \text{7-microphone probe.} \end{aligned} \tag{39}$$

The maximum normalized energy density for the one-dimensional sensor is given by either $1 - 0{\cdot}083(2kh)^2$ or 1 for the 2- and 3-microphone sensors respectively [5]. The minimum normalized energy density estimate is

$$\begin{aligned} \frac{E_{D_{min}}}{E_D} &= 1 - 0{\cdot}480(2kh), && \text{4-microphone probe without summer} \\ &= 1 - 0{\cdot}295(2kh) - 0{\cdot}150(2kh)^2, && \text{4-microphone probe with summer} \\ &= 1 - 0{\cdot}084(2kh)^2, && \text{6-microphone probe} \\ &= 1 - 0{\cdot}084(2kh)^2, && \text{7-microphone probe.} \end{aligned} \tag{40}$$

The minimum normalized energy density for the one-dimensional sensor is given by either $1 - 0{\cdot}250(2kh)^2$ or $1 - 0{\cdot}083(2kh)^2$ for the 2- and 3-microphone sensor respectively [5]. As expected, the maximum and minimum values of the normalized energy density of the 3-microphone sensor in a one-dimensional field are equal (within the accuracy of the simulation) to the maximum and minimum values for the 7-microphone sensor in three dimensions.

3.2.1.2. *Plane progressive wave.* The five measures of the accuracy of the energy density estimate for the four sensor configurations, as given by equations (30)–(34), are plotted in Figure 4. For the plane progressive wave it is quite apparent that the two models without the finite sum approximation, namely the 4-microphone sensor without the pressure summer and the 7-microphone sensor without the pressure summer (equations (22) and (28) respectively), out perform the two configurations which rely on the finite sum approximation. One may conclude that for free-field conditions the 4-microphone sensor without the summer will have a smaller inherent error than the 6-microphone sensor with the pressure summer. For real activities the sound field lies somewhere between a reactive sound field and a plane wave depending on the level of damping. Therefore, for acoustic systems which are heavily damped it is possible that the 4-microphone sensor without a pressure summer will have a smaller inherent error than the 6-microphone arrangement at high frequencies.

It was found that the normalized mean energy density for the four energy density sensor configurations converged to the following for large kh:

$$\begin{aligned}\frac{\bar{E}_D}{E_D} &= 1 - 0{\cdot}023(2kh)^2, \quad \text{4-microphone probe without summer}\\ &= 1 - 0{\cdot}107(2kh)^2, \quad \text{4-microphone probe with summer}\\ &= 1 - 0{\cdot}070(2kh)^2, \quad \text{6-microphone probe}\\ &= 1 - 0{\cdot}028(2kh)^2, \quad \text{7-microphone probe.}\end{aligned} \tag{41}$$

The normalized mean energy density for the one-dimensional sensor is either $1 - 0{\cdot}167(2kh)^2$ or $1 - 0{\cdot}042(2kh)^2$ for the 2- and 3-microphone sensor respectively [5]. It can be seen that the normalized r.m.s. error is given by

$$\begin{aligned}e(E_D)_{r.m.s.} &= 0{\cdot}024(2kh)^2, \quad \text{4-microphone probe without summer}\\ &= 0{\cdot}114(2kh)^2, \quad \text{4-microphone probe with summer}\\ &= 0{\cdot}071(2kh)^2, \quad \text{6-microphone probe}\\ &= 0{\cdot}030(2kh)^2, \quad \text{7-microphone probe.}\end{aligned} \tag{42}$$

The normalized standard deviation is given by

$$\begin{aligned}e(\bar{E}_D)_{r.m.s.} &= 0{\cdot}007(2kh)^2, \quad \text{4-microphone probe without summer}\\ &= 0{\cdot}038(2kh)^2, \quad \text{4-microphone probe with summer}\\ &= 0{\cdot}009(2kh)^2, \quad \text{6 and 7-microphone probes.}\end{aligned} \tag{43}$$

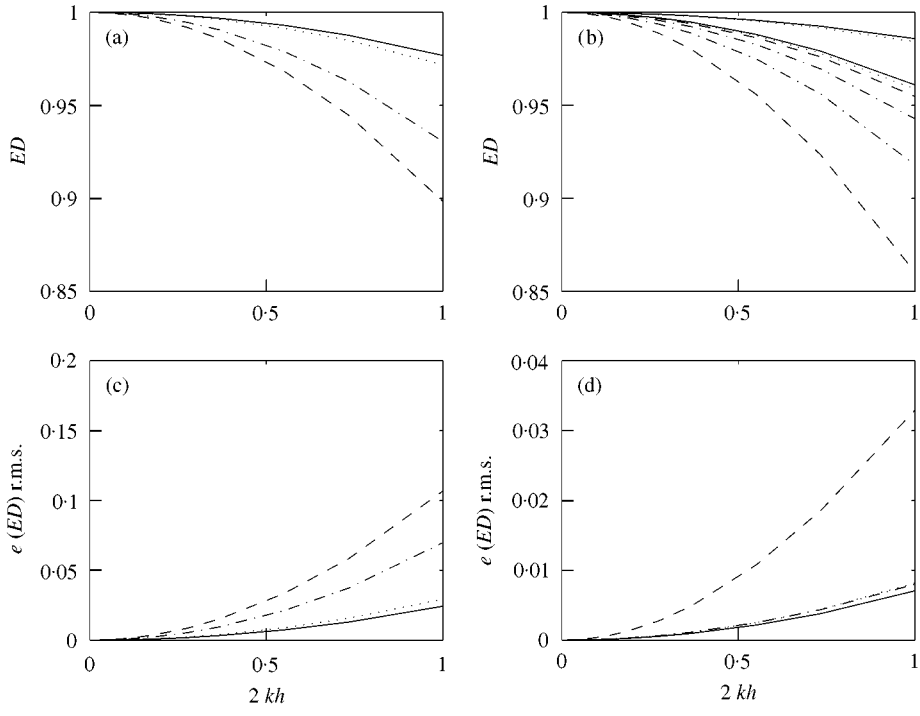

Figure 4. Inherent errors as a function of the non-dimensionalized separation distance $2kh$ for a plane progressive wave: (a) normalized mean energy density, (b) normalized maximum and minimum, (c) normalized r.m.s. error and (d) normalized standard deviation. —— 4 Mic; – – 4S Mic; ·–· 6 Mic; ···· 7 Mic.

The maximum normalized energy density estimate is

$$\frac{E_{D_{max}}}{E_D} = 1 - 0{\cdot}014(2kh)^2, \quad \text{4-microphone probe without summer}$$

$$= 1 - 0{\cdot}045(2kh)^2, \quad \text{4-microphone probe with summer}$$

$$= 1 - 0{\cdot}057(2kh)^2, \quad \text{6-microphone probe}$$

$$= 1 - 0{\cdot}016(2kh)^2, \quad \text{7-microphone probe.} \tag{44}$$

The minimum normalized energy density estimate is

$$\frac{E_{D_{min}}}{E_D} = 1 - 0{\cdot}039(2kh)^2, \quad \text{4-microphone probe without summer}$$

$$= 1 - 0{\cdot}150(2kh)^2, \quad \text{4-microphone probe with summer}$$

$$= 1 - 0{\cdot}084(2kh)^2, \quad \text{6-microphone probe}$$

$$= 1 - 0{\cdot}042(2kh)^2, \quad \text{7-microphone probe.} \tag{45}$$

Because the errors in the energy density estimates for the one-dimensional sensors in a plane wave are independent of position, the maximum and minimum are given by the mean energy density estimate.

3.2.2. *Phase mismatch*

The same two fields were analyzed with a phase shift imposed between the microphones. A phase difference of 1° has been used for the simulation and was chosen since it was found that most high-quality electret microphones will have phase errors of less than 1°. For the case of the 6- and 7-microphone sensors this meant a $\pm\frac{1}{2}^\circ$ shift with each pair. For the 4-microphone sensor, the "origin microphone" sensor was given a 1° phase shift. This was believed to be an acceptable approach to an error that would arise randomly.

3.2.2.1. *One-dimensional reactive field.* The five measures of the accuracy of the energy density estimate for the four-sensor configurations, as given by equations (30)–(34), arising from a 1° phase mismatch in a reactive sound field (for the four energy density sensor configurations) are plotted in Figure 5 for small kh.

It was found that the normalized mean energy density for all sensor configurations converged to the following for small wave numbers ($kh \leqslant \phi_s$):

$$\frac{\bar{E}_D}{E_D} = 1 + \frac{5}{3}\left(\frac{2\phi_s}{2kh}\right)^2, \tag{46}$$

where ϕ_s is in radians. It can be shown that the normalized mean energy density for both the one dimensional sensor is $1 + \frac{1}{2}((2\phi_s/2kh)^2$ [5]. Therefore, the bias error for all the three-dimensional sensors is $\frac{10}{3}$ times larger than the one-dimensional equivalent. The

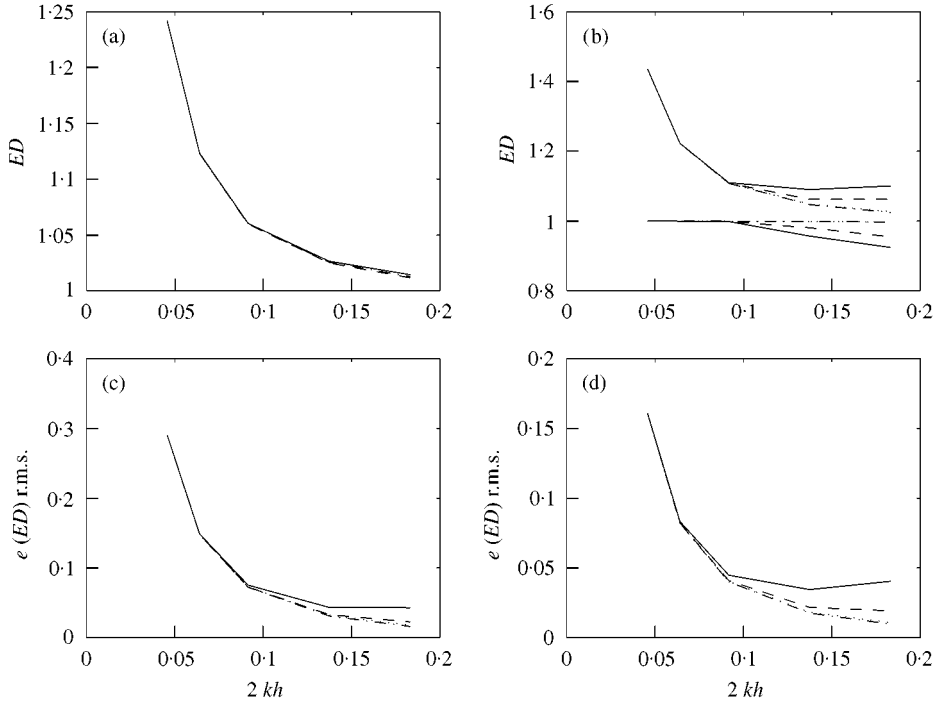

Figure 5. Normalized energy density error as a function of the non-dimensionalized separation distance $2kh$ for a phase mismatch of 1° between microphone pair in a reactive sound field: (a) normalized mean energy density, (b) normalized maximum and minimum, (c) normalized r.m.s. error and (d) normalized standard deviation. —— 4 Mic; – – 4S Mic; ·–· 6 Mic; ···· 7 Mic.

normalized r.m.s. error is given by

$$e(E_D)_{r.m.s.} = 2\left(\frac{2\phi_s}{2kh}\right)^2, \tag{47}$$

the normalized standard deviation, which gives a measure of the deviation about the mean, is given by

$$e(\bar{E}_D)_{r.m.s.} = \frac{\sqrt{11}}{3}\left(\frac{2\phi_s}{2kh}\right)^2 \tag{48}$$

and the maximum and minimum energy densities are, respectively, given by

$$\frac{E_{D_{max}}}{E_D} = 1 + 3\left(\frac{2\phi_s}{2kh}\right)^2 \tag{49}$$

and

$$\frac{E_{D_{min}}}{E_D} = 1. \tag{50}$$

The maximum energy density estimate for both the one-dimensional sensors is $1 + (2\phi_s/2kh)^2$ which is 3 times less than the maximum error for the three-dimensional sensors. The error in the minimum energy density estimate for the one-dimensional sensors is also zero [5].

3.2.2.2. *Plane progressive wave.* The five measures of the accuracy of the energy density estimate for the four sensor configurations, as given by equations (30)–(34), arising from a 1° phase mismatch in a progressive plane wave for the four energy density sensor configurations are plotted in Figure 6 for small *kh*.

It was found that the normalized mean energy density for the energy density sensor configurations converged to the following for small *kh*:

$$\frac{\bar{E}_D}{E_D} = 1 + \left(\frac{2\phi_s}{2kh}\right) + \frac{3}{2}\left(\frac{2\phi_s}{2kh}\right)^2, \quad \text{4-microphone probes}$$

$$= 1 - 0{\cdot}56\left(\frac{2\phi_s}{2kh}\right) + \frac{3}{2}\left(\frac{2\phi_s}{2kh}\right)^2, \quad \text{6 and 7-microphone probes} \tag{51}$$

The normalized mean energy density for the one-dimensional sensor is $1 - (2\phi_s/2kh) + \frac{1}{2}(2\phi_s/2kh)^2$ [5]. When $\phi_s < kh$ the mean energy density is given by the first two terms in the above expression and therefore the error for the 4-microphone sensors is approximately the same as the error arising for the one-dimensional sensors. The error for the 6- and 7-microphone sensor configurations is approximately half that of the one-dimensional sensors. However, as *kh* becomes very small, i.e., $\phi_s > kh$, the last term dominates and therefore, the error in the mean energy density estimate for the three-dimensional sensors is approximately 3 times larger than for the one-dimensional

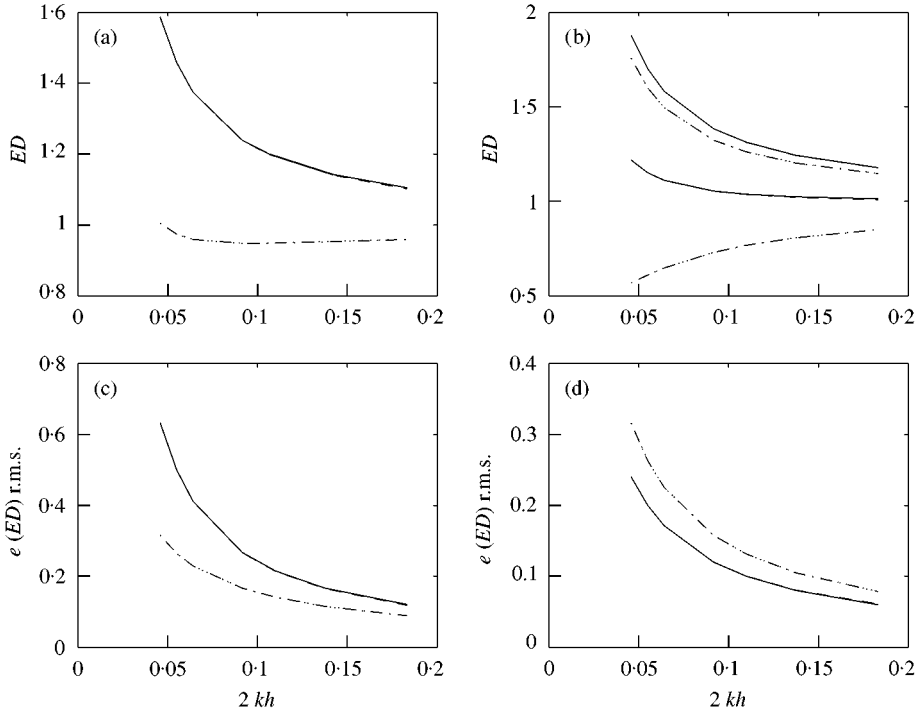

Figure 6. Normalized energy density errors as a function of the non-dimensionalized separation distance $2kh$ for a phase mismatch of 1° between microphone pairs in a plane progressive wave: (a) normalized mean energy density, (b) normalized maximum and minimum, (c) normalized r.m.s. error and (d) normalized standard deviation. —— 4 Mic; – – 4S Mic; ·–· 6 Mic; ···· 7 Mic.

sensors. The normalized r.m.s. error is given by

$$e(E_D)_{r.m.s.} = 1{\cdot}08\left(\frac{2\phi_s}{2kh}\right) + 1{\cdot}47\left(\frac{2\phi_s}{2kh}\right)^2, \quad \text{4-microphone probes}$$

$$= -0{\cdot}04\left(\frac{2\phi_s}{2kh}\right) + 1{\cdot}30\left(\frac{2\phi_s}{2kh}\right)^2, \quad \text{6 and 7-microphone probes,} \tag{52}$$

The normalized standard deviation is given by

$$e(\bar{E}_D)_{r.m.s.} = 0{\cdot}63\left(\frac{2\phi_s}{2kh}\right), \quad \text{4-microphone probes}$$

$$= 0{\cdot}83\left(\frac{2\phi_s}{2kh}\right), \quad \text{6 and 7-microphone probes.} \tag{53}$$

The maximum normalized energy density estimate is

$$\frac{E_{D_{max}}}{E_D} = 1 + \sqrt{3}\left(\frac{2\phi_s}{2kh}\right) + \frac{3}{2}\left(\frac{2\phi_s}{2kh}\right)^2, \quad \text{4-microphone probes}$$

$$= 1 + \sqrt{2}\left(\frac{2\phi_s}{2kh}\right) + \frac{3}{2}\left(\frac{2\phi_s}{2kh}\right)^2, \quad \text{6 and 7-microphone probes.} \tag{54}$$

The minimum normalized energy density estimate is

$$\frac{E_{D_{min}}}{E_D} = 1 + \frac{3}{2}\left(\frac{2\phi_s}{2kh}\right)^2, \quad \text{4-microphone probes}$$

$$= 1 - \left(1 + \frac{1}{\sqrt{2}}\right)\left(\frac{2\phi_s}{2kh}\right) + \frac{3}{2}\left(\frac{2\phi_s}{2kh}\right)^2, \quad \text{6- and 7-microphone probes,} \qquad (55)$$

For large kh, the energy density error due to a phase mismatch for both the reactive sound field and the propagating plane wave approaches zero and therefore the total error in the energy density is due wholly to the inherent errors.

3.2.3. *Sensitivity mismatch*

For the following analysis it has been assumed that the amplitudes of the individual microphone channels were calibrated to an accuracy of 1% between microphone pairs and that the cross-sensitivity was independent of frequency.

3.2.3.1. *One-dimensional reactive field.* The five measures of the accuracy of the energy density estimate for the four sensor configurations, as given by equations (30)–(34), arising from a 1% sensitivity mismatch for the four energy density sensor configurations are plotted in Figure 7 for small kh.

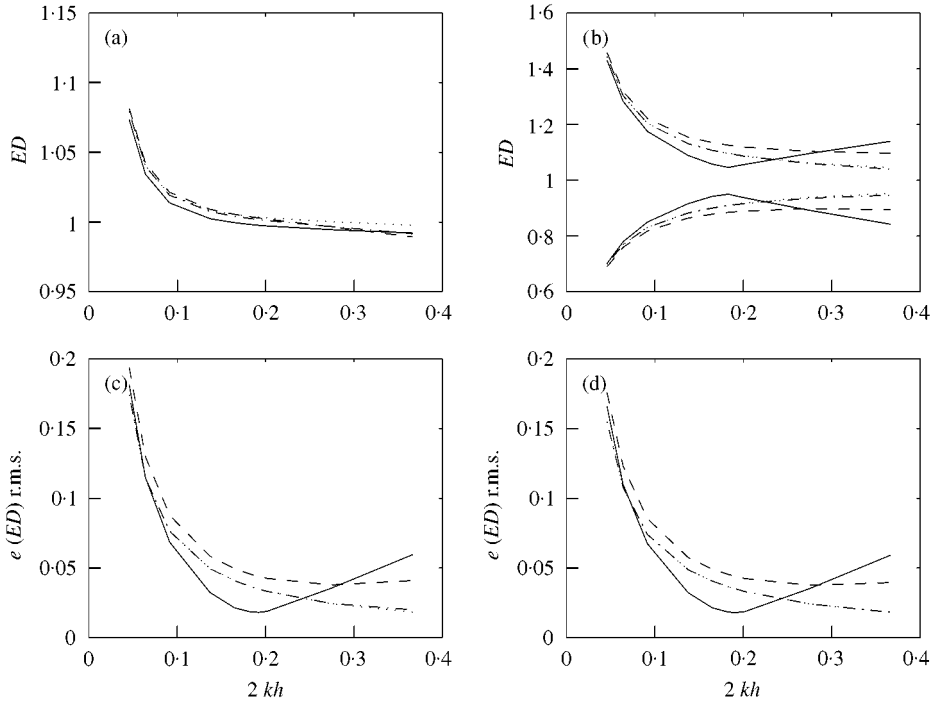

Figure 7. Normalized energy density errors as a function of the non-dimensionalized separation distance $2kh$ for a 1% sensitivity mismatch between microphone pair in a reactive sound field: (a) normalized mean energy density, (b) normalized maximum and minimum, (c) normalized r.m.s. error and (d) normalized standard deviation. —— 4 Mic; – – 4S Mic; · – · 6 Mic; ···· 7 Mic.

It was found that the normalized mean energy density for all the sensor configurations converged to the following for small kh:

$$\frac{\bar{E}_D}{E_D} = 1 + \frac{5}{3}\left(\frac{2T}{2kh}\right)^2. \tag{56}$$

The normalized r.m.s. error is given by

$$\begin{aligned} e(E_D)_{r.m.s.} &= 0{\cdot}33\left(\frac{2T}{2kh}\right) + 1{\cdot}81\left(\frac{2T}{2kh}\right)^2, \quad \text{4-microphone probe without summer} \\ &= 0{\cdot}36\left(\frac{2T}{2kh}\right) + 1{\cdot}79\left(\frac{2T}{2kh}\right)^2, \quad \text{4-microphone probe with summer} \\ &= 0{\cdot}28\left(\frac{2T}{2kh}\right) + 1{\cdot}84\left(\frac{2T}{2kh}\right)^2, \quad \text{6- and 7-microphone probes.} \end{aligned} \tag{57}$$

The normalized standard deviation is given by

$$\begin{aligned} e(\bar{E}_D)_{r.m.s.} &= 0{\cdot}50\left(\frac{2T}{2kh}\right) + 0{\cdot}84\left(\frac{2T}{2kh}\right)^2, \quad \text{4-microphone probe without summer} \\ &= 0{\cdot}52\left(\frac{2T}{2kh}\right) + 0{\cdot}83\left(\frac{2T}{2kh}\right)^2, \quad \text{4-microphone probe with summer} \\ &= 0{\cdot}42\left(\frac{2T}{2kh}\right) + 0{\cdot}88\left(\frac{2T}{2kh}\right)^2, \quad \text{6- and 7-microphone probes.} \end{aligned} \tag{58}$$

The maximum normalized energy density estimate is

$$\begin{aligned} \frac{E_{D_{max}}}{E_D} &= 1 + 1{\cdot}70\left(\frac{2T}{2kh}\right) + 1{\cdot}52\left(\frac{2T}{2kh}\right)^2, \quad \text{4-microphone probe without summer} \\ &= 1 + 1{\cdot}74\left(\frac{2T}{2kh}\right) + 1{\cdot}49\left(\frac{2T}{2kh}\right)^2, \quad \text{4-microphone probe with summer} \\ &= 1 + 1{\cdot}71\left(\frac{2T}{2kh}\right) + 1{\cdot}50\left(\frac{2T}{2kh}\right)^2, \quad \text{6- and 7-microphone probes.} \end{aligned} \tag{59}$$

The minimum normalized energy density estimate is

$$\begin{aligned} \frac{E_{D_{min}}}{E_D} &= 1 - 1{\cdot}72\left(\frac{2T}{2kh}\right) + 1{\cdot}50\left(\frac{2T}{2kh}\right)^2, \quad \text{4-microphone probe without summer} \\ &= 1 - 1{\cdot}73\left(\frac{2T}{2kh}\right) + 1{\cdot}50\left(\frac{2T}{2kh}\right)^2, \quad \text{4-microphone probe with summer} \\ &= 1 - 1{\cdot}71\left(\frac{2T}{2kh}\right) + 1{\cdot}50\left(\frac{2T}{2kh}\right)^2, \quad \text{6- and 7-microphone probes.} \end{aligned} \tag{60}$$

3.2.3.2. *Plane progressive wave.* The five measures of the accuracy of the energy density estimate for the four sensor configurations, as given by equations (30)–(34), arising from a 1% sensitivity mismatch for the four energy density sensor configurations are plotted in Figure 8 for small *kh*.

It was found that the mean normalized energy density for all sensor configurations converged to the following for small *kh*:

$$\frac{\bar{E}_D}{E_D} = 1 + \frac{3}{2}\left(\frac{2T}{2kh}\right)^2 \tag{61}$$

which is 3 times larger than for the one-dimensional case. The normalized r.m.s. error is given by

$$e(E_D)_{r.m.s.} = \frac{3}{2}\left(\frac{2T}{2kh}\right)^2, \tag{62}$$

the normalized standard deviation is given by

$$e(\bar{E}_D)_{r.m.s,} = 0 \tag{63}$$

and the maximum and minimum energy density are, respectively, given by

$$\frac{E_{D_{max}}}{E_D} = 1 + \frac{3}{2}\left(\frac{2T}{2kh}\right)^2 \tag{64}$$

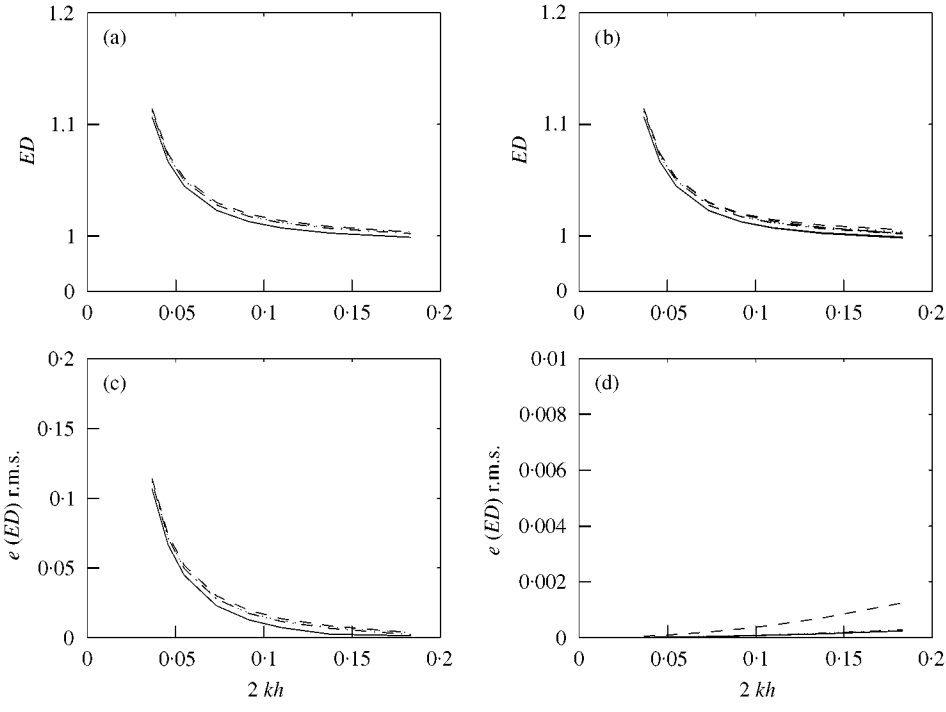

Figure 8. Normalized energy density errors as a function of the non-dimensionalised separation distance 2*kh* for a 1% sensitivity mismatch between microphone pairs in a plane progressive wave: (a) normalized mean energy density, (b) normalized maximum and minimum, (c) normalized r.m.s. error and (d) normalized standard deviation. —— 4 Mic; – – 4S Mic; · – · 6 Mic; ···· 7 Mic.

and

$$\frac{E_{D_{min}}}{E_D} = 1 + \frac{3}{2}\left(\frac{2T}{2kh}\right)^2. \tag{65}$$

For large kh the energy density error due to a sensitivity mismatch for both the reactive sound field and the propagating plane wave approaches zero and therefore the total error in the energy density is due wholly to the inherent errors.

3.2.4. *Spatial error*

The effect of spatial errors on the energy density estimate has been investigated. A 2 mm error between microphone pairs was used since it was typical of the spatial tolerance achievable. This was achieved by multiplying the original position matrices, defined by equations (5)–(7), by the ratio $(2 + 2h)/2h$, where h is in mm. This had the effect of stretching the physical positions of the microphone but was unaccounted for when calculating the pressure average and gradient.

3.2.4.1. *One-dimensional reactive field.* The five measures of the accuracy of the energy density estimate for the four-sensor configurations, as given by equations (30)–(34), arising from a 2 mm error between microphone pairs for the four energy density sensor configurations are plotted in Figure 9 for small kh. Since the bias errors arising from the spatial error at small kh are only a function of the non-dimensional spatial error ε/h (see below), it was necessary to keep ε/h constant. Figure 9 is therefore only valid for a non-dimensional spatial error of $\varepsilon/h = 4\%$ ($h = 5$ cm).

The variance of the error with respect to kh at high wavenumbers is associated with the inherent errors. At small kh it was found that the mean normalized energy density for all sensor configurations was independent of wavenumber and is given by the following:

$$\frac{\bar{E}_D}{E_D} = 1 + 0{\cdot}91\left(\frac{\varepsilon}{h}\right), \tag{66}$$

the normalized r.m.s. error is given by

$$e(E_D)_{r.m.s.} = 1{\cdot}18\left(\frac{\varepsilon}{h}\right), \tag{67}$$

the normalized standard deviational is given by

$$e(\bar{E}_D)_{r.m.s.} = 0{\cdot}75\left(\frac{\varepsilon}{h}\right), \tag{68}$$

and the maximum and minimum energy density are, respectively, given by

$$\frac{E_{D_{max}}}{E_D} = 1 + 2{\cdot}04\left(\frac{\varepsilon}{h}\right) \tag{69}$$

and

$$\frac{E_{D_{min}}}{E_D} = 1. \tag{70}$$

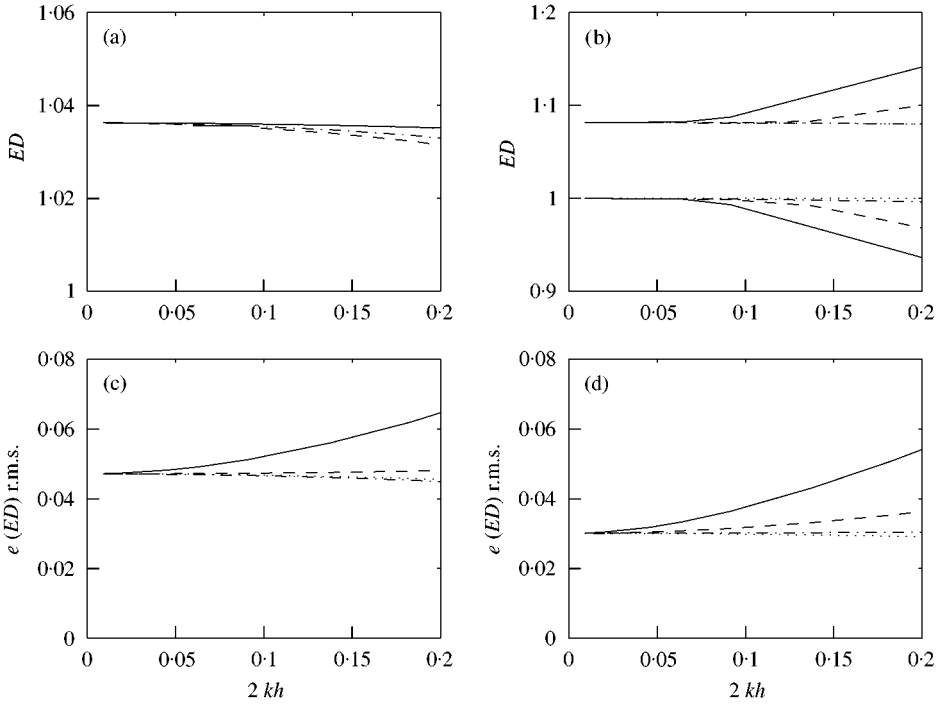

Figure 9. Normalized energy density errors as a function of the non-dimensionalized separation distance $2kh$ for a 2 mm spatial error between microphone pairs in a reactive sound field, i.e., $\varepsilon/h = 4\%$: (a) normalized mean energy density, (b) normalized maximum and minimum, (c) normalized r.m.s. error and (d) normalized standard deviation. —— 4 Mic; – – 4S Mic; ·–· 6 Mic; ···· 7 Mic.

All the plots in Figure 9 show finite separation effects as the non-dimensional separation ($2kh$) increases and is particularly apparent for $2kh$ greater than 0·05. Below a $2kh$ of 0·05 it can be seen that all the errors converge.

3.2.4.2. *Plane progressive wave.* The five measures of the accuracy of the energy density estimate for the four sensor configurations, as given by equations (30)–(34), arising from a 2 mm error between microphone pairs for the four energy density sensor configurations are plotted in Figure 10. As was the case with the reactive sound field, the bias errors arising from the spatial error are only a function of ε/h for small kh. Figure 10 is therefore only valid for $\varepsilon/h = 4\%$.

It was found that for small kh the mean normalized energy density for all probe configurations was given by the following:

$$\frac{E_D}{E_D} = 1 + \left(\frac{\varepsilon}{h}\right), \tag{71}$$

the normalized r.m.s. error is given by

$$e(E_D)_{r.m.s.} = \left(\frac{\varepsilon}{h}\right), \tag{72}$$

the normalized standard deviation is given by

$$e(\bar{E}_D)_{r.m.s.} = 0 \tag{73}$$

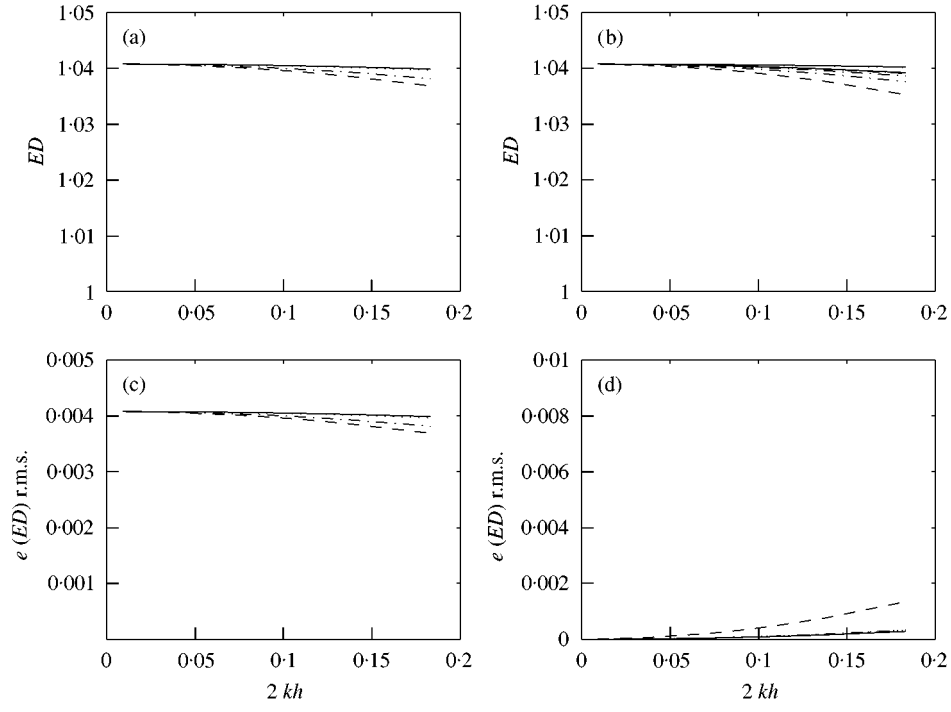

Figure 10. Normalized energy density errors as a function of the non-dimensionalized separation distance $2kh$ for a 2 mm spatial error between microphone pairs in a plane progressive wave, i.e., $\varepsilon/h = 4\%$: (a) normalized mean energy density, (b) normalized maximum and minimum, (c) normalized r.m.s. error and (d) normalized standard deviation. —— 4 Mic; – – 4S Mic; ·–· 6 Mic; ···· 7 Mic.

and the maximum and minimum energy density are, respectively, given by

$$\frac{E_{D_{max}}}{E_D} = \left(\frac{\varepsilon}{h}\right) \tag{74}$$

and

$$\frac{E_{D_{min}}}{E_D} = \left(\frac{\varepsilon}{h}\right) \tag{75}$$

This shows that the effect of a spatial error on the energy density estimate in a progressive plane wave is simply to bias the estimate by ε/h.

4. CONCLUSIONS

It has been shown that the energy density in both a one-dimensional reactive sound field and a plane wave can be measured adequately for active noise control applications using only 4-microphones rather than the 6 used conventionally.

The normalized errors in the energy density for all the 3-D sensor configurations converge to approximately the same value for the low-frequency limit in the idealized one-dimensional fields investigated here. This is to be expected since it has been shown in the companion paper [5] that the errors at the low-frequency limit are due to the finite

difference approximation of the velocity. The slight differences quoted here are most likely to be due to the finite step size used to integrate over all possible orientations.

It was found that for the low-frequency limit, the errors for the three-dimensional sensors were typically 3 times larger than were recorded for the one-dimensional sensors. This is due to the errors arising from each of the three axes adding to the total error. For the high-frequency limit, on the other hand, it was found that for both the reactive sound field and a plane wave, the errors for the three-dimensional sensors were less than the equivalent one-dimensional sensors. This is simply because the three-dimensional sensors provide a better estimate of both the pressure and velocities, but particularly the pressure, through better geometry.

When investigating the inherent errors in plane wave conditions, it was shown that at the high-frequency limit, the 4-microphone sensor without the summer performed significantly better than either the 4-microphone sensor with the summer or the 6-microphone sensor. This was because of the large errors associated with the finite sum used by the latter two sensor arrangements. The gain in performance was slightly offset by the reduction in performance at the low-frequency limit. Therefore, it may be concluded that the bandwidth of the 4-microphone sensor without a summer and the 6-microphone sensor in free-field conditions is approximately equal. The bandwidth of the 4-microphone sensor with the summer in the free field is less than the 4-microphone sensor without the summer. It may be argued that since the 4-microphone sensor without the summer is the simplest of the three sensor designs, it is the better arrangement for free-field control. The opposite holds in reactive conditions where the 6-microphone arrangement outperforms both of the 4-microphone energy density sensors.

Although the two sound fields used for the error analysis were one-dimensional they do provide an indication of the magnitudes of the errors that could be expected in fully three-dimensional sound fields. Since it has been shows that the magnitude of the energy density error is dependent on the wavelength of the sound field, it can be concluded that for a free-field environment composed of multiple plane waves the energy density error will be of a similar magnitude to that of a single plane wave. However, the situation for reactive sound fields is quite different since at any frequency there tends to be a dominant mode(s) which has a wavelength similar to the free-field wavelength (which is the same in 1-D and 3-D enclosures) and numerous higher order modes with shorter wavelengths. Even though these higher order modes have lower amplitudes than the dominant mode, it has been found that these higher order modes act to contaminate the energy density estimate and this is the subject of an on-going investigation [10, 11].

ACKNOWLEDGMENTS

The authors gratefully acknowledge the financial support for this work provided by Australian Research Council and the Sir Ross & Keith Smith Fund.

REFERENCES

1. S. D. SOMMERFELDT, J. W. PARKINS and Y. C. PARK 1995 *Proceedings of Active* 95, 477–488. Global active noise control in rectangular enclosures.
2. J. W. PARKINS, S. D. SOMMERFELDT and J. TICHY 1999 *Journal of the Acoustical Society of America*. Error analysis of a practical energy density sensor (accepted).
3. S. D. SOMMERFELDT and J. PARKINS 1994 *Journal of the Acoustical Society of America* **95**, 2989. Active control of energy density in three dimensional enclosures.

4. B. S. CAZZOLATO 1999 *Ph.D. dissertation, The University of Adelaide, March.* Sensing systems for active control of sound transmission into cavities.
5. B. S. CAZZOLATO and C. H. HANSEN 1999 *Journal of Sound and Vibration.* Errors in the measurement of acoustic energy density in one-dimensional sound fields (accepted).
6. G. W. ELKO 1991 *Proceedings of Noise-Con* 91, 525–533. An acoustic vector-field probe with calculable obstacle bias.
7. M. SCHUMACHER and E. L. HIXSON 1983 *Journal of the Acoustical Society of America* **74**, S62. A transducer and processing system to measure total acoustic energy density.
8. F. FAHY 1995 *Sound Intensity.* London: E&FN Spon. Second edition.
9. J. S. BENDAT and A. G. PIERSOL 1986 *Random Data—Analysis and Measurement Procedures.* New York: John Wiley & Sons. Second edition.
10. B. S. CAZZOLATO, C. D. KESTELL and C. H. HANSEN 1999 *Mechanical Engineering Technical Report No.* 1, *University of Adelaide.* Active noise control in a reactive duct with a virtual microphone and a virtual energy density sensor.
11. B. S. CAZZOLATO, C. D. KESTELL and C. H. HANSEN 1999 The effects of higher order mode on forward-difference virtual sensors (in preparation).